Study of Ageostrophy during Strong, Nonlinear Eddy-Front Interaction in the Gulf of Mexico

Luna Hiron, a David S. Nolan, a and Lynn K. Shaya

^a Rosenstiel School of Marine and Atmospheric Science, University of Miami, Miami, Florida

(Manuscript received 10 August 2020, in final form 10 December 2020)

ABSTRACT: The Loop Current (LC) system has long been assumed to be close to geostrophic balance despite its strong flow and the development of large meanders and strong frontal eddies during unstable phases. The region between the LC meanders and its frontal eddies was shown to have high Rossby numbers indicating nonlinearity; however, the effect of the nonlinear term on the flow has not been studied so far. In this study, the ageostrophy of the LC meanders is assessed using a high-resolution numerical model and geostrophic velocities from altimetry. A formula to compute the radius of curvature of the flow from the velocity field is also presented. The results indicate that during strong meandering, especially before and during LC shedding and in the presence of frontal eddies, the centrifugal force becomes as important as the Coriolis force and the pressure gradient force: LC meanders are in gradient-wind balance. The centrifugal force modulates the balance and modifies the flow speed, resulting in a subgeostrophic flow in the LC meander trough around the LC frontal eddies and supergeostrophic flow in the LC meander crest. The same pattern is found when correcting the geostrophic velocities from altimetry to account for the centrifugal force. The ageostrophic percentage in the cyclonic and anticyclonic meanders is $47\% \pm 1\%$ and $78\% \pm 8\%$ in the model and $31\% \pm 3\%$ and $78\% \pm 29\%$ in the altimetry dataset, respectively. Thus, the ageostrophic velocity is an important component of the LC flow and cannot be neglected when studying the LC system.

KEYWORDS: Ocean; Ageostrophic circulations; Eddies; Fronts; Mesoscale processes; Nonlinear dynamics

1. Introduction

Mesoscale eddies drive a large fraction of the variability in the ocean. Eddies with strong tangential velocity compared to their translation speed are able to stay coherent and travel long distances, carrying water mass properties, heat, nutrients, and particles around the ocean (McWilliams and Flierl 1979; Flierl 1981; Chelton et al. 2011; Haller and Beron-Vera 2013). The nonlinearity of these mesoscale features is greater for stronger flow and greater curvature, which, consequently, is associated with greater centrifugal force. Douglass and Richman (2015) showed that strong, nonlinear eddies in the Atlantic are in gradient-wind balance—they are governed by the pressure gradient force, the Coriolis force, and the centrifugal force. The ageostrophic flow associated with the centrifugal force was also studied by Kontoyiannis and Watts (1990) in the Gulf Stream using observations and by Chassignet and Xu (2017) in a high-resolution North Atlantic Ocean model. Kontoyiannis and Watts (1990) showed that the coalescence of cyclonic eddies with the stream increased the ageostrophic flow to values up to 30%-60% of the total observed velocity. Another study by Penven et al. (2014) showed that Mozambique Channel rings are also in gradient-wind balance.

In the Gulf of Mexico (GoM), a unique and very dynamic system has long been assumed to be in geostrophic balance. The Loop Current system is composed of the Loop Current (LC)—the only ocean current in the GoM, the Loop Current eddies (LCEs), and the Loop Current frontal eddies (LCFEs) (Fig. 1). The LC is a warm current flowing from the Caribbean Sea into the eastern GoM through the Yucatan Straits, turning anticyclonically, and exiting the GoM through the Florida

Corresponding author: Luna Hiron, lhiron@rsmas.miami.edu

Straits, where it gives origin to the Florida Current. When a maximum northward extension is reached, and the current becomes unstable, a warm eddy, or LCE, detaches from the LC, and flows southwestward toward Mexico at \sim 2.5–6 cm s⁻¹ (Lee and Mellor 2003; Schmitz 2005). The LC shedding is very irregular and occurs every 6-17 months (Vukovich 1988; Behringer et al. 1977; Sturges and Leben 2000). The detachment of the LCEs is one of the unsolved problems in the oceanographic community, and its prediction is still very inaccurate since many variables and forcings are associated with this process. On the other hand, it is known that the development of baroclinic instability is an important component as it leads to the formation and growth of the LC meanders before and during the LCE shedding (Hamilton et al. 2016; Donohue et al. 2016; Yang et al. 2020). Other processes such as the intrusion of Caribbean eddies and the increase in wind forcing (Oey et al. 2003) as well as the variability of the Yucatan Channel inflow (Ezer et al. 2003) have been shown to also influence the LC dynamics and shedding (Oey et al. 2005).

Baroclinic and barotropic instabilities in the LC drive the formation and amplification of frontal, cyclonic eddies in the vicinity of the LC: the LCFEs (Chérubin et al. 2006; Garcia-Jove et al. 2016; Yang et al. 2020). Strong frontal eddies have long been observed to play a role in the LCE detachment (Cochrane 1972; Vukovich et al. 1979; Vukovich and Maul 1985; Vukovich 1988; Lee et al. 1995; Fratantoni et al. 1998; Zavala-Hidalgo et al. 2003; Schmitz 2005). Linear and nonlinear interaction between the LCFE and the LC, and the advection of surrounding waters can cause further intensification and growth of the LCFEs, which leads to the enhancement of the LC meanders and, eventually, to the shedding of an LCE (Hiron et al. 2020). Intensified LCFEs have large negative sea surface height (SSH) (<-28 cm) and strong angular velocities, and they have been carefully characterized in Hiron et al. (2020).

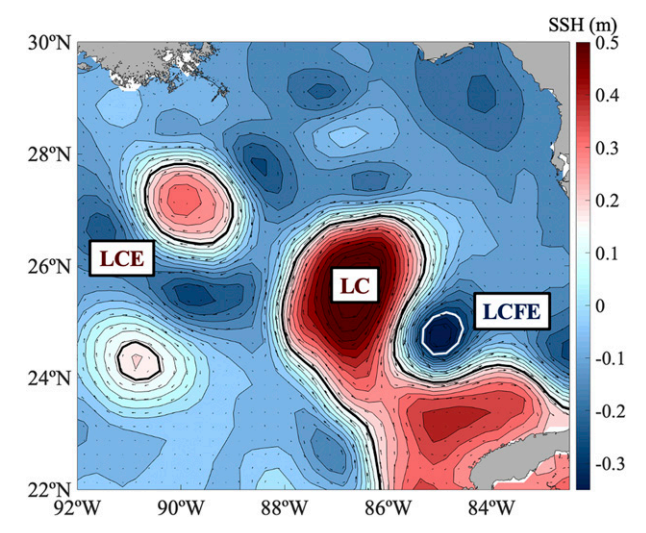


FIG. 1. SSH field from altimetry for the Loop Current system, which is composed of the Loop Current (LC), the Loop Current eddy (LCE), and the Loop Current frontal eddy (LCFE). The LC and LCE are shown by the 17-cm SSH black contour (Leben 2005) and the LCFE by the -28-cm SSH white contour (Hiron et al. 2020).

Other processes, such as vortex merging, vortex alignment, and vortex stretching, can also assist in the eddy intensification process (Cochrane 1972; Zavala-Hidalgo et al. 2003; Walker et al. 2011; Le Hénaff et al. 2012). As the LCFEs intensify and grow in size, their distance from the LC decreases, the LC meander amplifies, and the nonlinearity in the LC-LCFE front increases, reaching Rossby numbers greater than one (Hiron et al. 2020).

While the highly nonlinear aspect of the LC-LCFE interaction was explored in Hiron et al. (2020), the effect of ageostrophy on the flow has not been studied. This research aims first to evaluate if the LC meanders are gradient-wind balance and then, to understand how the ageostrophic term affects the flow. For systems in gradient-wind balance, the centrifugal force modulates the balance of forces, resulting in a subgeostrophic flow in cyclonic eddies and supergeostrophic in anticyclonic eddies (Wallace and Hobbs 2006). Here, the LC has an anticyclonic motion, whereas the LCFEs are cyclonic eddies, which makes the LC-LCFE interaction and the effect of the centrifugal force more complex.

For this study, we will apply the same method as Douglass and Richman (2015) to compute the gradient-wind velocity from the geostrophic velocity and the radius of curvature of the flow. Douglass and Richman (2015) only considered eddies with closed cores and high circularity, and the radius was computed from the area of the eddy. Our domain of interest is the LC meanders and, in particular, the LC-LCFE front; therefore, their method to compute the curvature cannot be applied. Instead, we use a formula from Cohen et al. (2019) that allows computing the radius of curvature of the flow from the velocity field around any given point.

This research presents the first study on the ageostrophic aspects of the LC system and presents a method to compute the radius of curvature of steady flows based on Cohen et al. (2019).

We use a high-resolution model to study the ageostrophic flow in the LC meanders during the last stages of the LC (preshedding and perishedding) and in the presence of an LCFE, which is when the LC meanders are sharper, and consequently, the centrifugal force is more important. We then apply the same method to altimetry data and show that the geostrophic velocities can be corrected to account for the effect of the centrifugal force.

2. Methodology

In this section, we first describe how the gradient-wind velocity can be calculated from the geostrophic velocity, as already done in previous studies. Then, we present the formula to calculate the radius of curvature of the flow around any given point.

a. Gradient-wind balance

The term "gradient wind" originated from meteorology (e.g., Kurita et al. 1985) and can be used interchangeably with "cyclogeostrophic." The gradient-wind balance is the balance between the centrifugal force, the Coriolis force and pressure-gradient force, and can be reduced to one equation by considering a natural coordinate system,

$$\frac{V_{\rm gr}^2}{R} + fV_{\rm gr} - g\frac{\partial \eta}{\partial R} = 0, \tag{1}$$

where $V_{\rm gr}$ is the magnitude of the gradient-wind velocity $(V_{\rm gr} = \sqrt{u_{\rm gr}^2 + v_{\rm gr}^2}), \, \eta$ is the SSH, f is the Coriolis parameter, and R is the radius of curvature of the flow. Equation (1) is valid for both anticyclonic and cyclonic flows and both hemispheres if R is defined positive for counterclockwise flow and negative for clockwise flow, i.e., positive for cyclonic and negative for anticyclonic motion in the North Hemisphere. If we replace $g(\partial \eta/\partial R) = fV_g$ (geostrophic balance), we can then express the gradient-wind balance as

$$\frac{V_{\rm gr}^2}{R} + fV_{\rm gr} - fV_{\rm g} = 0, (2)$$

where V_g is the magnitude of the geostrophic velocity $(V_g = \sqrt{u_g^2 + v_g^2})$. A useful form of the solution of the quadratic Eq. (2) for $V_{\rm gr}$ as a function of V_g is given by Knox and Ohmann (2006):

$$V_{\rm gr} = \frac{2V_g}{1 \pm \sqrt{1 + (4V_g/fR)}}.$$
 (3)

Equation (3) allows us to calculate the gradient-wind velocity from the geostrophic velocity. The positive solution is the one observed in most physical problems, as explained in Knox and Ohmann (2006), and is the one used here. Note that this equation has no real solution for anticyclonic flows (R < 0) with $|R| < 4V_g/f$. When R reaches this limit, $V_{\rm gr} = 2V_g$, which is the limit for stable flows. It can be shown that for $V_{\rm gr} > 2V_g$, we have $|\zeta_{\rm gr}| > f$, where $\zeta_{\rm gr}$ is the (negative) relative vorticity, which triggers inertial instability in the flow and violates the assumptions for gradient-wind balance (Knox 2003). On the

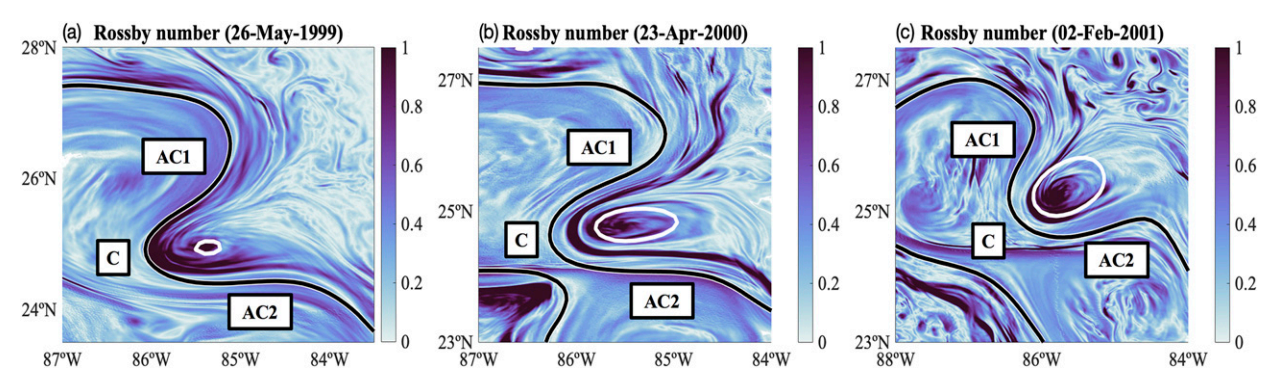


FIG. 2. Rossby number for the LC system on (a) 26 May 1999, (b) 23 Apr 2000, and (c) 2 Feb 2001 using HYCOM version 2.3.01. The 17- and -28-cm SSH contours are shown by the black and white lines, respectively. The letter C indicates the meander trough or cyclonic meander whereas AC1 and AC2 indicate the meander crests or anticyclonic meanders.

other hand, cyclonic flows have no limit as the square root is always positive and are free to intensify (e.g., hurricanes).

This method has been largely applied in the atmospheric field (Brill 2014; Thompson et al. 2018; Cohen et al. 2019). In oceanography, the study of the gradient-wind balance in ocean eddies has been less frequent, but Olson et al. (1985), Chassignet et al. (1990), Olson (1991), and more recently Penven et al. (2014), Douglass and Richman (2015), and Chassignet and Xu (2017), showed that strong, nonlinear eddies in the North Atlantic, the Mozambique Channel, and the Agulhas Current are in gradient-wind balance. The ageostrophic velocity associated with the centrifugal force is calculated by subtracting the geostrophic component of the flow from the gradient-wind velocity. The ageostrophic percentage of the flow is computed as

Ageo. (%) =
$$\left| 1 - \frac{V_{gr}}{V_g} \right| \times 100.$$
 (4)

The geostrophic velocity (u_g, v_g) is calculated using the SSH η field,

$$u_{g} = -\frac{g}{f} \frac{\partial \eta}{\partial y},$$

$$v_{g} = +\frac{g}{f} \frac{\partial \eta}{\partial x}.$$
(5)

Note that the gradient-wind velocity has the same orientation as the geostrophic velocity and can be stronger or weaker, dependent on the sign of the centrifugal force. The zonal and meridional components of the gradient-wind velocity (u_{gr}, v_{gr})

TABLE 1. Maximum Rossby number, gradient-wind velocity minus geostrophic velocity, and ageostrophic percentage for the Loop Current meander troughs and crests for three different cases using a high-resolution numerical model and altimetry dataset. The anticyclonic meanders 1 and 2 (AC1 and AC2) are the upstream and downstream meander crests, respectively, relative to the meander trough. The LC meander trough or cyclonic meander is indicated by C (or C1 and C2 when multiple). The location of the LC meander trough(s) and crests are shown in Fig. 2 and Fig. 7.

Dataset	Cases	Meander	R_o	Gradient-wind – geostrophic velocity (m s ⁻¹)	Ageostrophic percentage (%)
Model	26 May 1999	С	1.72	-1.00	46
	·	AC1	_	0.63	69
		AC2	_	0.76	66
	23 Apr 2000	C	3.70	-0.96	46
	•	AC1	_	0.73	80
		AC2	_	1.00	83
	2 Feb 2001	C	3.00	-1.48	48
		AC1	_	0.74	83
		AC2	_	0.57	84
Altimetry	10 Oct 2017	C	0.89	-0.37	33
		AC1	_	0.35	38
		AC2	_	0.71	99
	14 Apr 2018	C	1.00	-0.41	32
	•	AC1	_	0.78	90
		AC2	_	0.32	42
	29 May 2019	C1	0.97	-0.52	31
	·	C2	0.69	-0.30	27
		AC1	_	1.05	99
		AC2	_	0.73	97

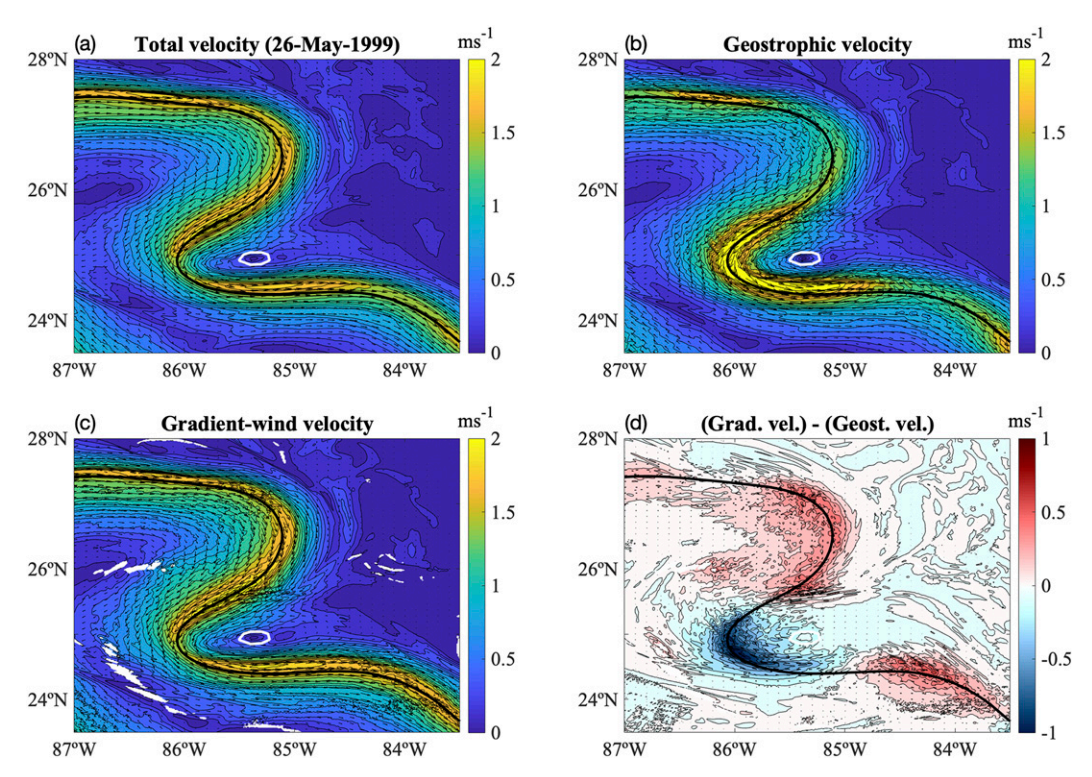


FIG. 3. Magnitude of (a) total velocity, (b) geostrophic velocity, (c) gradient-wind velocity, and (d) gradient-wind velocity minus geostrophic velocity, with their respective vectors, on 26 May 1999, a couple of weeks before LC shedding, using HYCOM version 2.3.01. The 17- and -28 cm SSH contours are shown by the black and white lines, respectively. The white patches in (c) show areas with undefined solutions due to small negative radius of curvature.

can be obtained by calculating the ratio between the gradientwind and the geostrophic velocity in natural coordinates, then multiplying this ratio by each component of the geostrophic velocity:

$$u_{\rm gr} = u_g \frac{V_{\rm gr}}{V_g},$$

$$v_{\rm gr} = v_g \frac{V_{\rm gr}}{V_g}.$$
 (6)

b. Radius of curvature of the flow

The main challenge to calculate the gradient-wind velocity is the computation of the radius of curvature. Following Cohen et al. (2019), the curl of a 2D vector field $\bf A$ can be expressed as the sum of the shear and the curvature of the flow in natural coordinates $\bf A$

$$\nabla \times \mathbf{A} = \hat{\mathbf{k}} \left(\frac{\partial A}{\partial \mathbf{n}} + \frac{A}{R} \right) \tag{7}$$

where $A = ||\mathbf{A}||$, $\hat{\mathbf{k}}$ is the vertical unit vector, and \mathbf{n} is the unit vector in the crosswind direction. Equation (7) is valid for steady flows, in which the trajectories are equal to the streamlines. We apply this equation to the 2D velocity field $\mathbf{v} = (u, v)$ and obtain the relative vorticity formula, which is

composed by the vorticity shear (first term) and the vorticity curvature (second term). If we divide the velocity field by its amplitude \mathbf{v} in the relative vorticity formula (7), the shear vanishes, and we obtain

$$R^{-1} = \hat{\mathbf{k}} \, \nabla \times \left(\frac{\mathbf{v}}{\|\mathbf{v}\|} \right). \tag{8}$$

Thus, for steady flows, the radius of curvature R is the inverse of the vertical component of the curl (i.e., the relative vorticity) of the unit vectors of \mathbf{v} . Using Eq. (8), R can be computed from the flow around any given point.

Alaka (1961) proposes a more complete formula to calculate the radius of curvature from the trajectories for flows in which the trajectories are different from the streamlines [Eqs. (14) and (15) in their paper]. For our case, the LCFEs translate at small velocities (Le Hénaff et al. 2014); therefore, we assume the trajectories to be equal to the streamlines and use the formula from Cohen et al. (2019).

3. Datasets

a. 1/100° free-run HYCOM

The Hybrid Coordinate Ocean Model (HYCOM) is a hybrid isopycnal–sigma-pressure coordinate ocean model (Bleck 2002; Chassignet et al. 2003), which uses isopycnal coordinates in the open, stratified ocean, sigma/terrain-following coordinates in

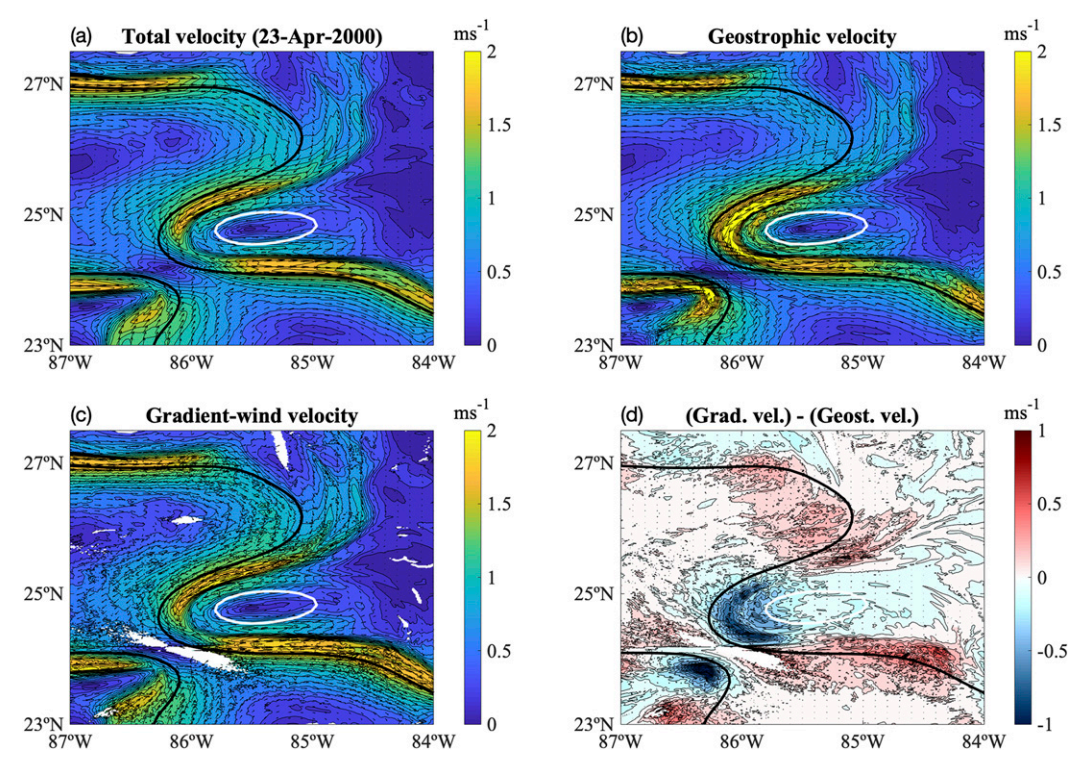


FIG. 4. As in Fig. 3, but for 23 Apr 2000, during LC shedding.

shallow coastal regions, and a pressure coordinate near the surface, in the mixed layer, and in unstratified seas. In this research, we use a 10-yr free-running Gulf of Mexico simulation (HYCOM version 2.3.01) forced by surface hourly wind fields provided by the Climate Forecast System Reanalysis (CFSR) atmospheric product for the 1994–2003 period, with turbulent flux and wind stress calculated following the Kara bulk formulation (Fairall et al. 2003; Kara et al. 2005) using absolute wind. The model is configured with the very high resolution (1/100°) Gulf of Mexico highresolution $(0.01^{\circ} \times 0.01^{\circ})$ bathymetric grid, version 2.0 (Velissariou 2014) and 41 vertical hybrid layers. The initial conditions (1 January 1994) as well as daily boundary conditions are provided by the HYCOM 1/12° (GOFS3.1) reanalysis available on the HYCOM website (https://www. hycom.org/dataserver/gofs-3pt1/reanalysis).

To match the SSH contours proposed by Leben (2005) and Hiron et al. (2020) to identify the LC (17 cm) and the LCFEs (-28 cm), respectively, we added a constant offset value of 0.15 cm to the modeled SSH. This ensures that the averaged mean model SSH is the same as Leben (2005) and Hiron et al. (2020) over the Gulf of Mexico and allows us to compare the contours that identify the LC and LCFE features in the figures.

b. AVISO+ SSH and geostrophic velocities

The reprocessed global ocean gridded L4 SSHs and derived variables (from 1993 to present) processes data from all altimeter missions (*Jason-3*, *Sentinel-3A*, *HY-2A*, *SARAL*/AltiKa, *Cryosat-2*, *Jason-2*, *Jason-1*, TOPEX/Poseidon,

Envisat, GFO, ERS-1/2), and was computed with respect to a 20-yr mean dynamic topography. This product has 1/4° resolution and is distributed by the Copernicus Marine and Environment Monitoring Service (CMEMS). In this study, we use the SSH above the geoid [i.e., the absolute dynamic topography (ADT)] and the associated geostrophic velocity.

The daily mean ADT over the Gulf of Mexico was subtracted from the ADT field following Leben (2005) to remove the seasonal variability of the upper ocean associated with thermal expansion and contraction. This mean is obtained by averaging the ADT for each day over the Gulf of Mexico deep water (>200 m). The absolute dynamic topography anomaly is herein referred to as SSH.

4. Nonlinearity in the LC-LCFE front

An indirect way to study ageostrophy is by quantifying the nonlinearity of the system. Hiron et al. (2020) noted an increase in the Rossby number in the LC–LCFE front as the LCFE intensified. To evaluate if the model used in this study captures the nonlinearity of the LC–LCFE front, we calculated the Rossby number for the LC system for three different cases of strong LC meandering in the presence of LCFE: one case (26 May 1999) a couple of weeks before a LC shedding and two other cases (23 April 2000 and 2 February 2001) during LC shedding (Fig. 2). We define the Rossby number R_o as the absolute value of the ratio between the relative vorticity ω and the Coriolis parameter f,

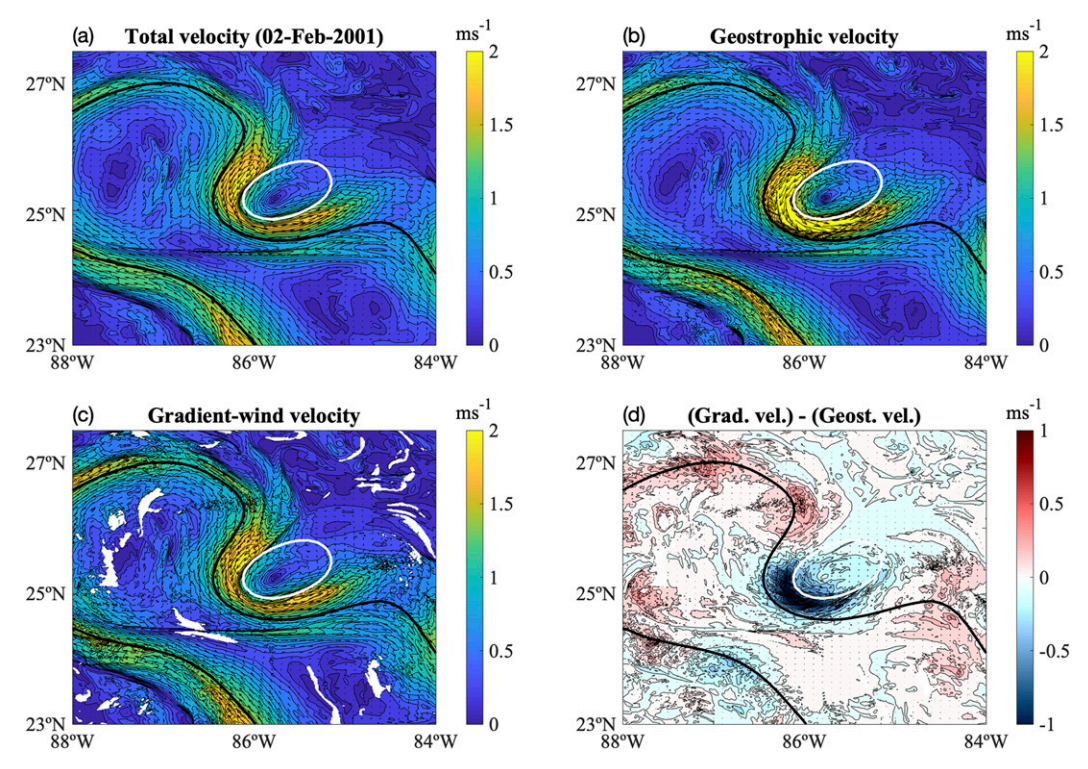


FIG. 5. As in Fig. 3, but for 2 Feb 2001, during LC shedding.

$$R_o = \left| \frac{\omega}{f} \right|$$
.

A small R_o (~0.1) indicates that the nonlinear term in the momentum budget equation is small compared to the Coriolis force and, therefore, can be neglected. In this case, the system is potentially in geostrophic balance. On the other hand, high R_o (\sim 1) shows that the nonlinear term is as important as the Coriolis force, and therefore cannot be neglected. In the model, the center of the LC appears to have low R_o . The LC front, on the other hand, is more nonlinear. We observe high values (~1) in many places around the LC front, but most importantly, we note an area of high nonlinearity between the LC and the intensified LCFE with values of R_o exceeding 1 for the three cases. We found maximum R_o values of 1.72, 3.70, and 3.00 between the LC and the LCFE for the three cases, respectively (Fig. 2) and Table 1). This result confirms the increase in nonlinearity in the LC-LCFE front during eddy intensification, in agreement with Hiron et al. (2020).

The geostrophic balance is, among others, based on the assumption that the flow is slow and relatively straight. For regions with strong flows and high curvature, the centrifugal force becomes important, and the flow is no longer in geostrophic balance. The LC is very strong, with velocities reaching up to 1.7 m s⁻¹ (Forristall et al. 1992), and meanders with high curvature are common, especially during the last stages of the LC when baroclinic instability is important (Hamilton et al. 2016; Donohue et al. 2016; Yang et al. 2020). The last stages of the LC include the period before and during

the shedding of an LCE. The intensification of LCFEs leads to further growth of the meanders and can participate in the shedding of the LC. Thus, high Rossby numbers in regions of strong LC meandering indicates that the centrifugal force is

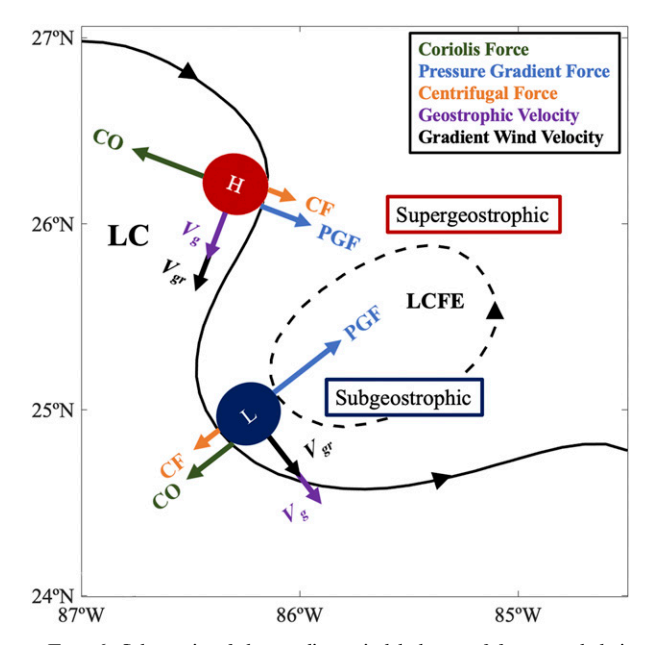


FIG. 6. Schematic of the gradient-wind balance of forces and their effects on the geostrophic and gradient-wind velocity in the Loop Current meanders around high (H) and low (L) pressure centers. The solid line represents the LC boundary, and the dashed line represents an LCFE.

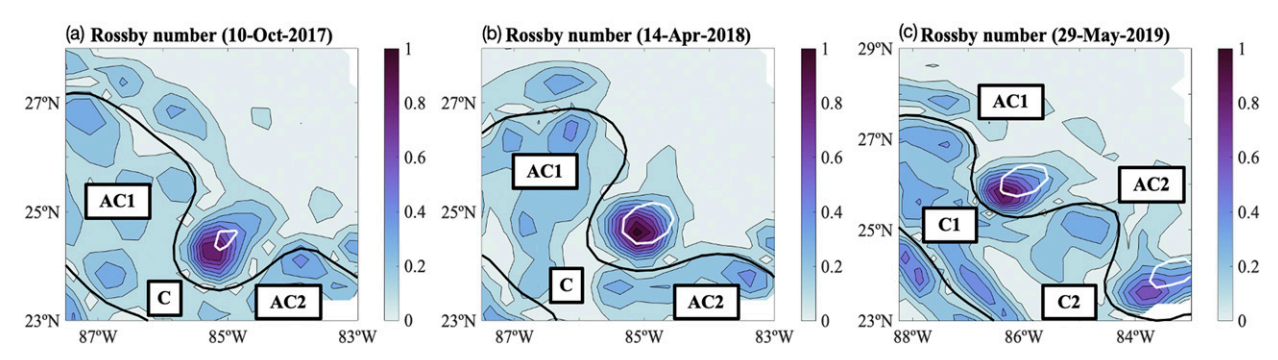


FIG. 7. Rossby number for the LC system on (a) 10 Oct 2017, (b) 14 Apr 2018, and (c) 29 May 2019 using geostrophic velocity from altimetry. The 17- and -28-cm SSH contours are shown by the black and white lines, respectively. The letter C indicates the meander trough or cyclonic meander (C1 and C2 when multiple cyclonic meanders appear), whereas AC1 and AC2 indicate the meander crests or anticyclonic meanders.

important. The next section will evaluate the impact of the centrifugal force on the LC meanders.

5. Gradient-wind balance before and during LC shedding and eddy intensification: Model perspective

The geostrophic velocity and the gradient-wind velocity were computed following section 2 using the high-resolution HYCOM for the three different cases of strong LC meandering discussed in section 4 (Figs. 3–5). For the three cases, the LC

front is strong in particular around the LCFE, with values reaching 2 m s⁻¹ (Figs. 3a, 4a, and 5a). The geostrophic velocity is even stronger than the total velocity in the meander trough around the LCFE, with values reaching 2.6, 2.8, and 3 m s⁻¹ (Figs. 3b, 4b, and 5b, respectively). On the other hand, the geostrophic velocity is slightly weaker in the meander crest compared to the total velocity. The "meander trough" is the portion of the LC meander having a cyclonic motion, around the LCFE, and the "meander crest" is the portion of the LC meander with an anticyclonic motion above the meander

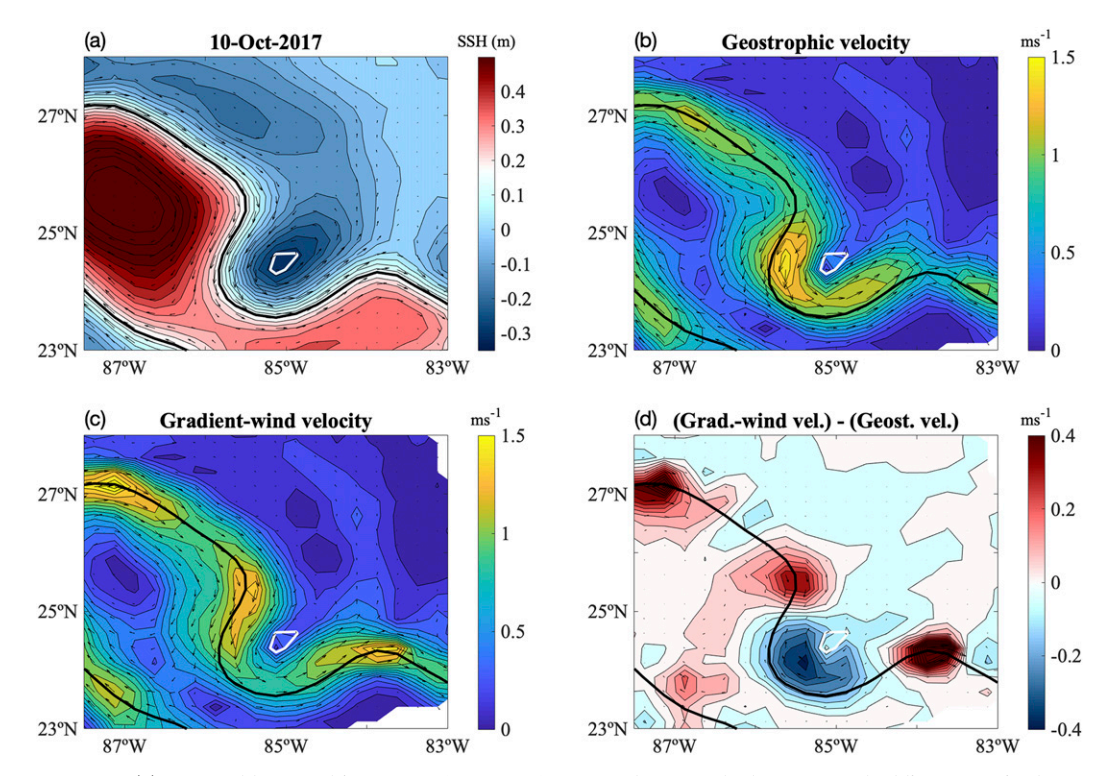


FIG. 8. (a) SSH field from altimetry on 10 Oct 2017, a couple of weeks before LC shedding. Magnitude of (b) geostrophic velocity, (c) gradient-wind velocity, and (d) gradient-wind velocity minus geostrophic velocity, with their respective vectors. The 17- and -28-cm SSH contours are shown by the black and white lines, respectively.

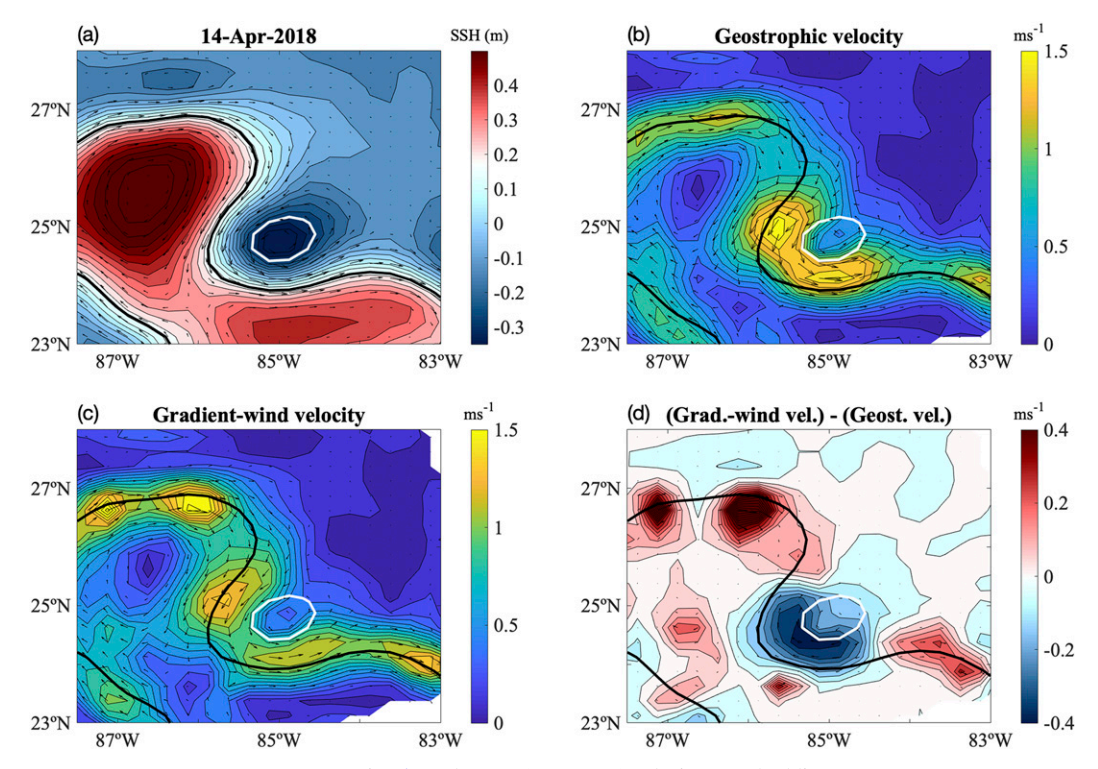


FIG. 9. As in Fig. 8, but for 14 Apr 2018, during LC shedding.

trough. In most cases, a second meander crest forms below the meander trough. For systems in gradient-wind balance, the geostrophic velocity overestimates cyclonic flows and underestimates anticyclonic flows. In fact, the gradient-wind velocity is very similar to the total velocity for the three cases (Figs. 3c, 4c, and 5c), which confirms that the LC meanders are in gradient-wind balance. Note that the white patches show areas with undefined solutions due to small negative radius of curvature. The difference between the gradient-wind velocity and the geostrophic velocity (Figs. 3d, 4d, and 5d and Table 1) averaged among the three cases indicates that the ageostrophic component strengthens the flow by $0.74 \pm 0.15 \,\mathrm{m\,s^{-1}}$ in the meander crest and weakens it by $1.15 \pm 0.29 \,\mathrm{m\,s^{-1}}$ in the meander trough. The values of velocity discussed here are in reference to the maximum values in the LC meander crests and trough.

The strength of the ageostrophic component associated with the centrifugal force is dependent on the strength and the radius of curvature of the flow. We display in Table 1 the values of the ageostrophic percentage [Eq. (4)] for the locations where the ageostrophic flow reaches its maximum in the cyclonic and the anticyclonic meanders. For the model analysis, the ageostrophic velocity averaged among the three cases consists of $47\% \pm 1\%$ of the geostrophic velocity in the cyclonic meander and of $78\% \pm 8\%$ in the anticyclonic meanders. These values were obtained by finding the maximum ageostrophic velocity for each cyclonic and anticyclonic meanders. For the three cases, the residual (i.e., the difference between the total velocity and the gradient-wind velocity) is smaller than $0.2\,\mathrm{m\,s^{-1}}$ in the LC meander

trough and crests. As a comparison, Douglass and Richman (2015) found the ageostrophic velocity corresponded to 21% of the geostrophic velocity for the cyclonic eddy, and 53% for the anticyclonic eddy.

The centrifugal force is always directed outward from the rotational motion and modifies the balance of force differently depending on its orientation relative to the pressure gradient force and the Coriolis force. As predicted by the gradient-wind theory, the flow in the LC meander trough around the LCFE is subgeostrophic, whereas the flow in the LC meander crests is supergeostrophic. The schematic in Fig. 6 summarizes the balance of forces in the LC meanders in the presence of an intensified LCFE.

6. Application to geostrophic velocities from altimetry

The gradient-wind method can be applied to geostrophic velocities from altimetry, as done by Penven et al. (2014) and Douglass and Richman (2015). The Rossby number and the gradient-wind velocity were computed for three cases of strong LC meandering in the presence of LCFE: one case during LC shedding (14 April 2018) and two others a couple of weeks before LC shedding (10 October 2017 and 29 May 2019). For the 2019 case, a second trough formed in association with another LCFE. Since the geostrophic velocity and the gradient-wind velocity have the same direction, the radius of curvature of the flow can be computed from the geostrophic velocity.

For the three cases, the area between the LC and the LCFEs presented high R_o values: 0.89 and 1.00 for the 2017 and 2018

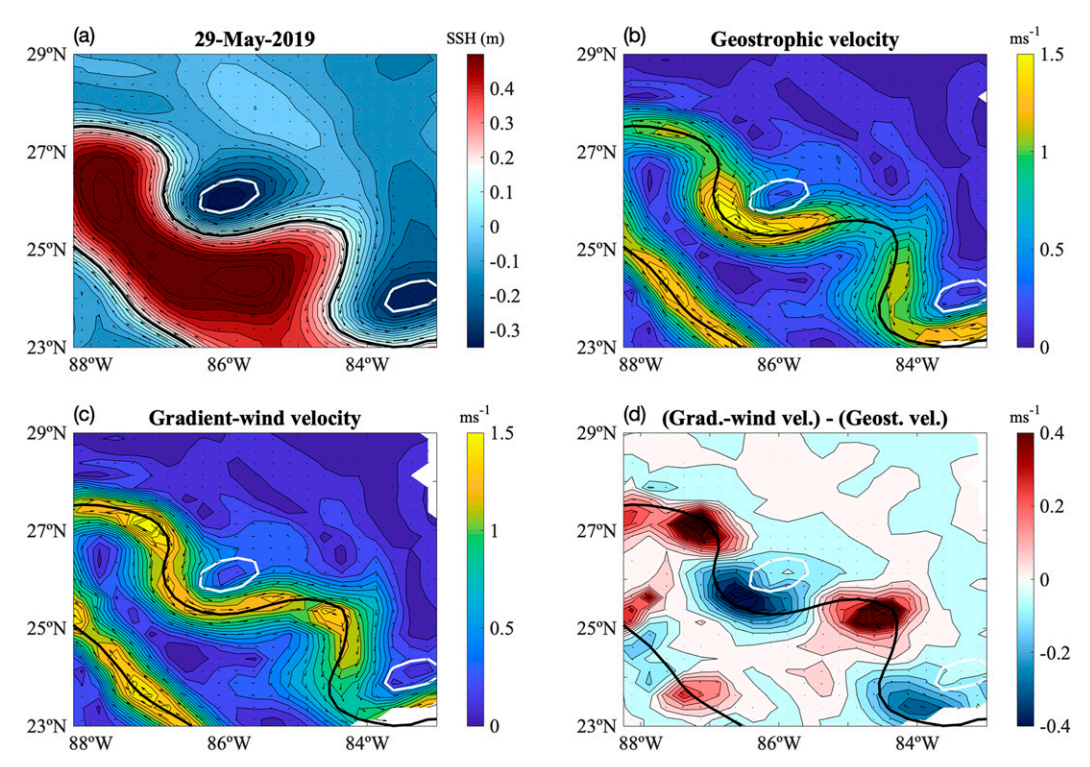


Fig. 10. As in Fig. 8, but for 29 May 2019, a couple of weeks before LC shedding.

cases, respectively, and 0.97 and 0.69 for the upper and lower troughs for the 2019 case, respectively (Fig. 7 and Table 1), and coincides with the locations of high nonlinearity in the model (Fig. 2). The gradient-wind velocity, the geostrophic velocity, and the difference between the two velocities for the three cases have similar patterns as the model output but with smaller magnitudes (Figs. 8–10). The smaller velocity magnitude in the altimetry dataset is partially due to the smoothing and the coarse resolution of the SSH field. On average, the gradient-wind velocity is slower than the geostrophic velocity in the LC meander trough ($-0.4 \pm 0.09 \,\mathrm{m\,s^{-1}}$) and faster than the geostrophic velocity in the LC meander crest ($0.66 \pm 0.28 \,\mathrm{m\,s^{-1}}$) (Table 1 and Figs. 8d, 9d, and 10d). The ageostrophic velocity consists of $31\% \pm 3\%$ of the geostrophic velocity in the cyclonic meander and of $78\% \pm 29\%$ in the anticyclonic meander (Table 1).

7. Conclusions

This study demonstrates the importance of the centrifugal force in the LC meanders using a high-resolution numerical model and geostrophic velocity from altimetry. During the last stages of the LC, before and during shedding, LC meanders get sharper in particular due to the intensification of frontal eddies. During these stages, the centrifugal force is as important as the Coriolis force and the pressure-gradient force, i.e., the LC meanders are in gradient-wind balance. The centrifugal force modulates the balance and modifies the flow speed, resulting in a subgeostrophic flow in the LC meander trough around the LCFE and supergeostrophic flow in the LC meander crest, following the gradient-wind theory.

For the model analysis, the ageostrophic velocity averaged among the three cases consists of $47\% \pm 1\%$ of the geostrophic velocity in the cyclonic meander and of $78\% \pm 8\%$ in the anticyclonic meanders. Since the gradient-wind velocity can be calculated from the geostrophic velocity, data from altimetry can be corrected to account for the effects of the centrifugal force. We applied this technique to an altimetry dataset, and we obtained similar patterns for the effect of the centrifugal force as the one obtained with the model. For the altimetry dataset, the ageostrophic flow associated with the centrifugal force is of $31\% \pm 3\%$ in the cyclonic meander and of $78\% \pm 29\%$ in the anticyclonic meander.

These findings highlight the importance of measuring the total velocity, e.g., from techniques such as APEX-EM floats (Shay et al. 2019) or high-frequency (HF) radars (Shay et al. 2007), to avoid overestimating/underestimating the flow in the LC meanders. The ageostrophic velocity is an important component of the LC flow and, therefore, cannot be neglected when studying the LC system.

Acknowledgments. The authors thank Eric P. Chassignet and Alexandra Bozec for providing the high-resolution HYCOM output and for their useful comments on this manuscript, and to Yair Cohen for the discussions on the computation of the radius of curvature. L. Hiron also thanks Homar V. Ortega for the interesting discussions at the 2020 Ocean Sciences Meeting. This study has been conducted using E.U. Copernicus Marine Service Information (https://marine.copernicus.eu). This research is made possible by the Gulf of Mexico Research Initiative through Grant 2015-V-487 made to the University of

Miami. LKS also acknowledges partial support from National Academies of Sciences, Engineering and Medicine: Understanding Gulf Ocean Systems-1: Dry Tortugas and Lower Keys High Frequency Radars Grant to the University of South Florida through a subcontract to the University of Miami (2500-1745-00-B).

REFERENCES

- Alaka, M. A., 1961: The occurrence of anomalous winds and their significance. *Mon. Wea. Rev.*, **89**, 482–494, https://doi.org/10.1175/1520-0493(1961)089<0482:TOOAWA>2.0.CO;2.
- Behringer, D. W., R. L. Molinari, and J. F. Festa, 1977: The variability of anticyclonic current patterns in the Gulf of Mexico. J. Geophys. Res., 82, 5469–5476, https://doi.org/ 10.1029/JC082i034p05469.
- Bleck, R., 2002: An oceanic general circulation model framed in hybrid isopycnic-Cartesian coordinates. *Ocean Modell.*, **4**, 55–88, https://doi.org/10.1016/S1463-5003(01)00012-9.
- Brill, K., 2014: Revisiting an old concept: The gradient wind. Mon. Wea. Rev., 142, 1460–1471, https://doi.org/10.1175/ MWR-D-13-00088.1.
- Chassignet, E. P., and X. Xu, 2017: Impact of horizontal resolution (1/12° to 1/50°) on Gulf Stream separation, penetration, and variability. J. Phys. Oceanogr., 47, 1999–2021, https://doi.org/ 10.1175/JPO-D-17-0031.1.
- ——, D. B. Olson, and D. B. Boudra, 1990: Motion and evolution of oceanic rings in a numerical model and in observations.
 J. Geophys. Res., 95, 22121–22140, https://doi.org/10.1029/JC095iC12p22121.
- —, L. T. Smith, G. R. Halliwell, and R. Bleck, 2003: North Atlantic simulations with the Hybrid Coordinate Ocean Model (HYCOM): Impact of the vertical coordinate choice, reference pressure, and thermobaricity. *J. Phys. Oceanogr.*, 33, 2504–2526, https://doi.org/10.1175/1520-0485(2003)033<2504: NASWTH>2.0.CO;2.
- Chelton, D. B., M. G. Schlax, and R. M. Samelson, 2011: Global observations of nonlinear mesoscale eddies. *Prog. Oceanogr.*, 91, 167–216, https://doi.org/10.1016/j.pocean.2011.01.002.
- Chérubin, L. M., Y. Morel, and E. P. Chassignet, 2006: Loop Current ring shedding: The formation of cyclones and the effect of topography. *J. Phys. Oceanogr.*, 36, 569–591, https:// doi.org/10.1175/JPO2871.1.
- Cochrane, J. D., 1972: Separation of an anticyclone and subsequent developments in the Loop Current. Contributions on the Physical Oceanography of the Gulf of Mexico, Gulf Publishing Co., 91–106.
- Cohen, Y., S. L. Durden, N. Harnik, and E. Heifetz, 2019: Relating observations of gradient nonbalance at the top of hurricanes with their warm core structures. *Geophys. Res. Lett.*, 46, 11510–11519, https://doi.org/10.1029/2019GL084248.
- Donohue, K. A., D. R. Watts, P. Hamilton, R. Leben, and M. Kennelly, 2016: Loop Current eddy formation and baroclinic instability. *Dyn. Atmos. Oceans*, 76, 195–216, https:// doi.org/10.1016/j.dynatmoce.2016.01.004.
- Douglass, E. M., and J. G. Richman, 2015: Analysis of ageostrophy in strong surface eddies in the Atlantic Ocean. J. Geophys. Res. Oceans, 120, 1490–1507, https://doi.org/10.1002/2014JC010350.
- Ezer, T., L.-Y. Ocy, W. Sturges, and H.-C. Lee, 2003: The variability of currents in the Yucatan Channel: Analysis of results from a numerical ocean model. *J. Geophys. Res.*, 108, 3012, https://doi.org/10.1029/2002JC001509.

- Fairall, C. W., E. F. Bradley, J. E. Hare, A. A. Grachev, and J. B. Edson, 2003: Bulk parameterization of air–sea fluxes: Updates and verification for the COARE algorithm. *J. Climate*, **16**, 571–591, https://doi.org/10.1175/1520-0442(2003)016<0571: BPOASF>2.0.CO;2.
- Flierl, G. R., 1981: Particle motions in large-amplitude wave fields. Geophys. Astrophys. Fluid Dyn., 18, 39–74, https://doi.org/ 10.1080/03091928108208773.
- Forristall, G. Z., K. J. Schaudt, and C. K. Cooper, 1992: Evolution and kinematics of a Loop Current eddy in the Gulf of Mexico during 1985. J. Geophys. Res., 97, 2173–2184, https://doi.org/ 10.1029/91JC02905.
- Fratantoni, P. S., T. N. Lee, G. P. Podesta, and F. Muller-Karger, 1998: The influence of Loop Current perturbations on the formation and evolution of Tortugas eddies in the southern Straits of Florida. *J. Geophys. Res.*, **103**, 24759–24779, https://doi.org/10.1029/98JC02147.
- Garcia-Jove, M., J. Sheinbaum, and J. Jouanno, 2016: Sensitivity of Loop Current metrics and eddy detachments to different model configurations: The impact of topography and Caribbean perturbations. *Atmoisfera*, 29, 235–265, https://doi.org/10.20937/ ATM.2016.29.03.05.
- Haller, G., and F. Beron-Vera, 2013: Coherent Lagrangian vortices: The black holes of turbulence. J. Fluid Mech., 731, R4, https://doi.org/10.1017/jfm.2013.391.
- Hamilton, P., A. Lugo-Fernández, and J. Sheinbaum, 2016: A Loop Current experiment: Field and remote measurements. *Dyn. Atmos. Oceans*, 76, 156–173, https://doi.org/ 10.1016/j.dynatmoce.2016.01.005.
- Hiron, L., B. Jaimes de la Cruz, and L. K. Shay, 2020: Evidence of Loop Current frontal eddy intensification through local linear and nonlinear interactions with the Loop Current. *J. Geophys. Res. Oceans*, 125, e2019JC015533, https://doi.org/ 10.1029/2019JC015533.
- Kara, A. B., H. E. Hurlburt, and A. J. Wallcraft, 2005: Stability-dependent exchange coefficients for air–sea fluxes. *J. Atmos. Oceanic Technol.*, 22, 1080–1094, https://doi.org/10.1175/JTECH1747.1.
- Knox, J. A., 2003: Inertial instability. Encyclopedia of the Atmospheric Sciences, J. R. Holton, J. Pyle, and J. A. Curry, Eds., Elsevier, 1004–1013.
- —, and P. R. Ohmann, 2006: Iterative solutions of the gradient wind equation. *Comput. Geosci.*, 32, 656–662, https://doi.org/ 10.1016/j.cageo.2005.09.009.
- Kontoyiannis, H., and D. R. Watts, 1990: Ageostrophy and pressure work in the Gulf stream at 73°W. *J. Geophys. Res.*, **95**, 22 209–22 228, https://doi.org/10.1029/JC095iC12p22209.
- Kurita, H., K. Sasaki, H. Muroga, H. Ueda, and S. Wakamatsu, 1985: Long-range transport of air pollution under light gradient wind conditions. J. Climate Appl. Meteor., 24, 425–434, https://doi.org/ 10.1175/1520-0450(1985)024<0425:LRTOAP>2.0.CO;2.
- Le Hénaff, M., V. H. Kourafalou, Y. Morel, and A. Srinivasan, 2012: Simulating the dynamics and intensification of cyclonic Loop Current frontal eddies in the Gulf of Mexico. *J. Geophys. Res.*, **117**, C02034, https://doi.org/10.1029/2011JC007279.
- —, —, R. Dussurget, and R. Lumpkin, 2014: Cyclonic activity in the eastern Gulf of Mexico: Characterization from along-track altimetry and in situ drifter trajectories. *Prog. Oceanogr.*, 120, 120–138, https://doi.org/10.1016/j.pocean.2013.08.002.
- Leben, R. R., 2005: Altimeter-derived Loop Current metrics. Circulation in the Gulf of Mexico: Observations and Models, Geophys. Monogr., Vol. 161, Amer. Geophys. Union, 181–202, https://doi.org/10.1029/161GM15.

- Lee, H.-C., and G. L. Mellor, 2003: Numerical simulation of the Gulf Stream System: The Loop Current and the deep circulation. *J. Geophys. Res.*, **108**, 3043, https://doi.org/10.1029/2001JC001074.
- Lee, T. N., K. Leaman, E. Williams, T. Berger, and L. Atkinson, 1995: Florida current meanders and gyre formation in the southern Straits of Florida. J. Geophys. Res., 100, 8607–8620, https://doi.org/10.1029/94JC02795.
- McWilliams, J. C., and G. R. Flierl, 1979: On the evolution of isolated, nonlinear vortices. *J. Phys. Oceanogr.*, 9, 1155–1182, https://doi.org/10.1175/1520-0485(1979)009<1155:OTEOIN>2.0.CO;2.
- Oey, L.-Y., H.-C. Lee, and W. J. Schmitz Jr., 2003: Effects of winds and Caribbean eddies on the frequency of Loop Current eddy shedding: A numerical model study. J. Geophys. Res., 108, 3324, https://doi.org/10.1029/2002JC001698.
- —, T. Ezer, and H.-C. Lee, 2005: Loop Current, rings and related circulation in the Gulf of Mexico: A review of numerical models and future challenges. *Circulation in the Gulf of Mexico: Observations and Models*, *Geophys. Monogr.*, Vol. 161, Amer. Geophys. Union, 31–56, https://doi.org/doi:10.1029/161GM04.
- Olson, D. B., 1991: Rings in the ocean. *Annu. Rev. Earth Planet. Sci.*, **19**, 283–311, https://doi.org/10.1146/annurev.ea.19.050191.001435.
- —, R. W. Schmitt, M. A. Kennelly, and T. M. Joyce, 1985: A two-layer diagnostic model of the long term physical evolution of warm core ring 82-B. *J. Geophys. Res.*, 90, 8813–8822, https://doi.org/10.1029/JC090iC05p08813.
- Penven, P., I. Halo, S. Pous, and L. Marié, 2014: Cyclogeostrophic balance in the Mozambique channel. *J. Geophys. Res. Oceans*, **119**, 1054–1067, https://doi.org/10.1002/2013JC009528.
- Schmitz, W. J., Jr., 2005: Cyclones and westward propagation in the shedding of anticyclonic rings from the Loop Current. Circulation in the Gulf of Mexico: Observations and Models, Geophys. Monogr., Vol. 161, Amer. Geophys. Union, 241–261, https://doi.org/10.1029/161GM18.
- Shay, L. K., J. Martinez-Pedraja, T. M. Cook, B. K. Haus, and R. H. Weisberg, 2007: High-frequency radar mapping of surface currents using WERA. *J. Atmos. Oceanic Technol.*, 24, 484–503, https://doi.org/10.1175/JTECH1985.1.
- —, J. Brewster, B. Jaimes, C. Gordon, K. Fennel, P. Furze, H. Fargher, and R. He, 2019: Physical and biochemical variability

- from APEX-EM floats. *Proc. 12th IEEE/OES Current, Waves and Turbulence Measurement*, San Diego, CA, IEEE, 6 pp., https://doi.org/10.1109/CWTM43797.2019.8955168.
- Sturges, W., and R. Leben, 2000: Frequency of ring separations from the Loop Current in the Gulf of Mexico: A revised estimate. *J. Phys. Oceanogr.*, **30**, 1814–1819, https://doi.org/10.1175/1520-0485(2000)030<1814:FORSFT>2.0.CO;2.
- Thompson, C. F., D. M. Schultz, and G. Vaughan, 2018: A global climatology of tropospheric inertial instability. *J. Atmos. Sci.*, **75**, 805–825, https://doi.org/10.1175/JAS-D-17-0062.1.
- Velissariou, P. 2014: Gulf of Mexico high-resolution (0.01° x 0.01°) bathymetric grid version 2.0. Gulf of Mexico Research Initiative Information and Data Cooperative, Harte Research Institute, Texas A&M University–Corpus Christi, accessed 15 June 2020, https://doi.org/10.7266/N7X63JZ5.
- Vukovich, F. M., 1988: Loop Current boundary variations. J. Geophys. Res., 93, 15585–15591, https://doi.org/10.1029/JC093iC12p15585.
- —, and G. A. Maul, 1985: Cyclonic eddies in the eastern Gulf of Mexico. J. Phys. Oceanogr., 15, 105–117, https://doi.org/ 10.1175/1520-0485(1985)015<0105:CEITEG>2.0.CO;2.
- ——, B. W. Crissman, M. Bushnell, and W. J. King, 1979: Some aspects of the oceanography of the Gulf of Mexico using satellite and in situ data. *J. Geophys. Res.*, 84, 7749–7768, https://doi.org/10.1029/JC084iC12p07749.
- Walker, N. D., and Coauthors, 2011: Impacts of Loop Current frontal cyclonic eddies and wind forcing on the 2010 Gulf of Mexico oil spill. Monitoring and Modeling the Deepwater Horizon Oil Spill: A Record-Breaking Enterprise, Geophys. Monogr., Vol. 195, Amer. Geophys. Union, 103–116, https:// doi.org/10.1029/2011GM001120.
- Wallace, J. M., and P. V. Hobbs, 2006: Atmospheric Science: An Introductory Survey. 2nd ed. Elsevier, 504 pp.
- Yang, Y., R. H. Weisberg, Y. Liu, and X. S. Liang, 2020: Instabilities and multiscale interactions underlying the Loop Current eddy shedding in the Gulf of Mexico. *J. Phys. Oceanogr.*, **50**, 1289–1317, https://doi.org/10.1175/JPO-D-19-0202.1.
- Zavala-Hidalgo, J., S. L. Morey, and J. J. O'Brien, 2003: Cyclonic eddies northeast of the Campeche Bank from altimetry data. *J. Phys. Oceanogr.*, **33**, 623–629, https://doi.org/10.1175/1520-0485(2003)033<0623:CENOTC>2.0.CO;2.